Progress In Electromagnetics Research, PIER 34, 1–27, 2001

SCATTERING OF AN $E_{//}$-POLARIZED PLANE WAVE BY ONE-DIMENSIONAL ROUGH SURFACES: NUMERICAL APPLICABILITY DOMAIN OF A RAYLEIGH METHOD IN THE FAR-FIELD ZONE

C. Baudier and R. Dusséaux

Université de Versailles Saint-Quentin en Yvelines
Centre d'étude des Environnements Terrestre et Planétaires (CETP)
10-12, avenue de l'Europe, 78140 Vélizy, France

Abstract—The field scattered by a perfectly conducting plane surface with a perturbation illuminated by an $E_{//}$-polarized plane wave is determined by means of a Rayleigh method. This cylindrical surface is described by a local function. The scattered field is supposed to be represented everywhere in space by a superposition of a continuous spectrum of outgoing plane waves. A "triangle/Dirac" method of moments applied to the Dirichlet boundary condition in the spectral domain allows the wave amplitudes to be obtained. For a half cosine arch, the proposed Rayleigh method is numerically investigated in the far-field zone, by means of convergence tests on the spectral amplitudes and on the power balance criterion. We show that the Rayleigh integral can be used for perturbations, the amplitudes of which are close to half the wavelength.

1. INTRODUCTION

We propose to determine, by means of a Rayleigh method, the field scattered by a perfectly conducting plane surface with a cylindrical local deformation illuminated by an $E_{//}$-polarized plane wave. The surface is defined by the equation $y = a(x)$, where $a(x)$ is a local function. Above the deformation, the scattered field can be represented by a superposition of a continuous spectrum of outgoing plane waves [1, 2], the so called Rayleigh integral. The amplitudes of these propagating and evanescent plane waves are given by the function $\hat{c}(\alpha)$, where integration variable α represents the propagation constant in the x direction. The Rayleigh integral is assumed to be valid everywhere in space, outside and on the surface (Section 2). Once the Rayleigh hypothesis assumed, a "triangle/Dirac" moment method [3, 4] applied to the Dirichlet boundary condition in the spectral domain allows function $\hat{c}(\alpha)$ to be obtained. First, function $\hat{c}(\alpha)$ is decomposed on a basis of triangle functions $\hat{b}_p(\alpha)$ with variable supports. Then, to compute the expansion coefficients c_p, the Fourier transform of the boundary condition is used at many discrete values of α (Section 3).

The theoretical validity of the Rayleigh hypothesis has given rise to some work for rough surfaces [1, 2] and for diffraction gratings [5–17]. If $a(x)$ is not analytical, the Rayleigh hypothesis is generally not valid. For an analytical profile, the calculation of the theoretical validity bounds follows from the location of the singularities of the representation of the exterior scattered field [5–13]. The Rayleigh hypothesis is only valid for weakly modulated surfaces. Two classical results can be mentioned: for a perfectly conducting grating defined by $a(x) = (h/2)\cos(2\pi x/D)$ in $E_{//}$-polarization, the assumption does not hold if $\pi h/D > 0.448$ [5–7]. For profile $a(x) = h\sin(x)/x$ with the Dirichlet condition, the Rayleigh integral can define the scattered field if $-1.1161 < h < 0.98537$ [1].

In practice, numerical experiments show that it is possible to obtain reliable results in the far zone, even outside the theoretical validity domain [3, 10–12]. For the grating example above, the values of the efficiencies are reliable for $\pi h/D \lesssim 2$ (i.e., a numerical applicability domain about 4.5 times wider than the theoretical validity domain).

Recent work has revived the interest of Rayleigh methods. M. Bagieu and D. Maystre have applied a well-adapted regularization process to the Rayleigh-Fourier method for gratings [13, 14]. This process does not modify the theoretical validity domain of the Rayleigh expansion but allows one to extend, in an efficient way, the numerical applicability domain in the far-field zone. A. I. Kleev and A. B. Manenkov prove that with an adaptive collocation method, the Rayleigh series are fully capable of describing the field produced by gratings or cylindrical objects for which the Rayleigh hypothesis is not valid [15–17].

This paper does not deal with the theoretical validity bounds of the Rayleigh hypothesis. Its main purpose is to define the numerical applicability domain of the proposed Rayleigh method, in the far zone and for non-analytical profiles. This investigation uses convergence tests on expansion coefficients c_p and on the power balance criterion. A comparison with a rigorous method is made (Section 4).

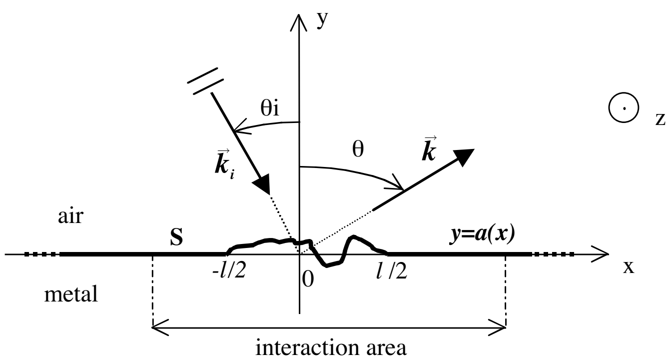

Figure 1. Plane with a local deformation illuminated by a plane wave with incidence angle θ_i. According to our conventions, θ_i and θ are positive here.

2. FORMULATION OF THE PROBLEM AND RAYLEIGH INTEGRAL

We consider a cylindrical rough surface S which is invariant along the z-axis (Fig. 1). This surface is a plane with a local deformation. Its profile is described by the function $y = a(x)$ with a finite support:

$$a(x) = 0 \qquad \text{if} \qquad x \notin [-l/2; l/2] \tag{1}$$

Surface S separates the air ($y > a(x)$) from a perfectly conducting metal ($y < a(x)$). S is illuminated by an $E_{//}$-polarized electromagnetic monochromatic plane wave. Its wave-vector $\vec{k}_i$ is lying in the xOy plane ($\left\|\vec{k}_i\right\| = k = 2\pi/\lambda$) and forms an angle θ_i with Oy.

Without any deformation ($a(x) = 0$), the scattering phenomenon is restricted to specular reflection. Using the time dependence factor $e^{j\omega t}$, the complex vectors of the fields are:

$$\vec{E}_t^{(0)}(x,y) = \vec{E}_i(x,y) + \vec{E}_r(x,y) \qquad \forall y \geq a(x)$$
$$\text{where} \begin{cases} \vec{E}_i(x,y) = E_i(x,y)\vec{u}_z = e^{-j\alpha_i x + j\beta_i y}\vec{u}_z \\ \vec{E}_r(x,y) = E_r(x,y)\vec{u}_z = -e^{-j\alpha_i x - j\beta_i y}\vec{u}_z \end{cases} \text{with} \begin{cases} \alpha_i = k\sin\theta_i \\ \beta_i = k\cos\theta_i \end{cases} \tag{2}$$

"t", "i" and "r" indices are associated with the total, incident and reflected fields, respectively. The incident and reflected plane waves have an infinite power and a finite mean power density per unit surface:

$$\begin{aligned} &\frac{1}{2}\mathrm{Re}\left[\int_0^1\int_{-\infty}^{+\infty}\left(\vec{E}_{\substack{i\\r}}(x,y)\wedge\vec{H}^*_{\substack{i\\r}}(x,y)\right)\cdot\vec{u}_y dxdz\right] \to \infty \\ &\frac{1}{2}\mathrm{Re}\left[\lim_{\Delta x\to+\infty}\frac{1}{\Delta x}\int_0^1\int_{-\Delta x/2}^{+\Delta x/2}\left(\vec{E}_{\substack{i\\r}}(x,y)\wedge\vec{H}^*_{\substack{i\\r}}(x,y)\right)\cdot\vec{u}_y dxdz\right] < \infty \end{aligned} \tag{3}$$

The plane being locally deformed ($a(x) \neq 0$ when $x \in [-l/2; l/2]$), we consider, in addition to the incident and reflected waves, a scattered wave ($\vec{E}_d, \vec{H}_d$) such that:

$$\vec{E}_t(x,y) = \vec{E}_t^{(0)}(x,y) + \vec{E}_d(x,y) \qquad \forall y \geq a(x) \tag{4}$$

$$\begin{aligned} &\frac{1}{2}\mathrm{Re}\left[\int_0^1\int_{-\infty}^{+\infty}\left(\vec{E}_d(x,y)\wedge\vec{H}^*_d(x,y)\right)\cdot\vec{u}_y dxdz\right] < \infty \\ &\frac{1}{2}\mathrm{Re}\left[\lim_{\Delta x\to+\infty}\frac{1}{\Delta x}\int_0^1\int_{-\Delta x/2}^{+\Delta x/2}\left(\vec{E}_d(x,y)\wedge\vec{H}^*_d(x,y)\right)\cdot\vec{u}_y dxdz\right] = 0 \end{aligned} \tag{5}$$

The incident wave generates on S surface currents which radiate in the air by behaving like secondary sources. The scattered wave corresponds to the wave which is radiated only by the "interaction area". This area is the zone of S including the deformation and a small area near the deformation (Fig. 1). According to the concept of weak coupling [18, 19], the surface current at a point P of S only depends on the shape of the profile within a circle having its center at P and a radius of up to several wavelengths. This principle implies that the surface current far from the deformation only generates the reflected wave.

The interaction area receives a finite incident power. Therefore, the scattered wave must have a finite power and a zero mean power density per unit surface (5).

Let $y_{\max}$ be the maximum height of the deformation ($y_{\max} = \max[a(x)]$ when $x \in]-\infty;+\infty[$). Field $E_d(x,y)$ satisfies the Helmholtz equation $\Delta E_d(x,y) + k^2 E_d(x,y) = 0$ for all $y \geq a(x)$. In the area where $y > y_{\max}$, an exact solution of this equation, which also satisfies the outgoing wave condition, is a continuum of plane waves, the so-called Rayleigh integral:

$$E_d(x,y) = \frac{1}{2\pi} \int_{-\infty}^{+\infty} \hat{c}(\alpha) e^{-j\beta(\alpha)y} e^{-j\alpha x} d\alpha \qquad \begin{cases} \forall x \in]-\infty;+\infty[\\ \forall y > y_{\max} \end{cases}$$
$$\text{with} \quad \begin{cases} \beta(\alpha) = \sqrt{(k^2-\alpha^2)} & \text{if } |\alpha| \leq k \\ \beta(\alpha) = -j\sqrt{(\alpha^2-k^2)} & \text{if } |\alpha| > k \end{cases} \tag{6}$$

When $|\alpha| > k$, $\beta(\alpha)$ is a pure imaginary value and the corresponding waves are evanescent waves. Otherwise, $\beta(\alpha)$ is real and the waves are propagating. In both cases, an angular representation of α and $\beta(\alpha)$ is used:

$$\text{if } |\alpha| \leq k: \{\alpha = k\sin\theta \text{ and } \beta(\alpha) = k\cos\theta \text{ with } \theta \in [-\pi/2;\pi/2]$$
$$\text{if } |\alpha| > k: \begin{cases} \text{if } \alpha > k: & \alpha = k\cosh\theta \text{ and } \beta(\alpha) = -jk\sinh\theta \text{ with } \theta > 0 \\ \text{if } \alpha < -k: & \alpha = -k\cosh\theta \text{ and } \beta(\alpha) = jk\sinh\theta \text{ with } \theta < 0 \end{cases} \tag{7}$$

We demonstrate in the appendix that Rayleigh integral (6) in the far-field zone can be reduced to:

$$\begin{cases} \vec{E}_d(r,\varphi) \approx \dfrac{e^{-jkr}}{\sqrt{r}} \sqrt{\dfrac{k}{2\pi}} e^{j\pi/4} \hat{c}(\varphi) \cos\varphi \vec{u}_z \\ \vec{H}_d(r,\varphi) \approx -\dfrac{1}{Z} \dfrac{e^{-jkr}}{\sqrt{r}} \sqrt{\dfrac{k}{2\pi}} e^{j\pi/4} \hat{c}(\varphi) \cos\varphi \vec{u}_\varphi \end{cases} \tag{8}$$

with $Z = \sqrt{\mu_0/\varepsilon_0} \approx 120\pi$, and with polar coordinates (r,φ) such that $x = r\sin\varphi$ and $y = r\cos\varphi$. The electric and magnetic fields decrease as $1/\sqrt{r}$ in the far-field zone [20]. The angular dependence is given by the function $\hat{c}(\varphi)\cos\varphi$.

Using (8), the scattered elementary power $dP_d(\theta)$ is defined:

$$\frac{dP_d(\theta)}{d\theta} = \frac{k}{4\pi Z} |\hat{c}(\theta)|^2 \cos^2\theta \qquad \forall \theta \in]-\pi/2;\pi/2[\tag{9}$$

$dP_d(\theta)$ is the real part of the flux of the complex scattered Poynting vector through the elementary surface $d\vec{S} = rd\varphi\Delta z\vec{u}_r$ where $\varphi = \theta$ with $\Delta z = 1$. $dP_d(\theta)/d\theta$ is the angular (scattered) power density. This function defines the scattering pattern.

Function $\hat{c}(\theta)$ verifies the power balance criterion [18, 21, 22]:

$$P_d = P_c \text{ with } P_d = \int_{\theta=-\pi/2}^{+\pi/2} dP_d(\theta) \quad \text{and} \quad P_c = \frac{1}{Z}\mathrm{Re}[\hat{c}(\theta_i)]\cos\theta_i \quad (10)$$

where P_d is the total scattered power and P_c represents the electromagnetic coupling between the incident, reflected and scattered waves.

We want to determine the field $E_d(x, y)$ in the far-field zone and the angular power density $dP_d(\theta)/d\theta$: therefore the amplitudes $\hat{c}(\alpha)$ of the propagating waves in the Rayleigh integral must be obtained. The proposed method uses the Dirichlet boundary condition on S with the help of a "triangle/Dirac" moment method [3, 4]. The originality resides in the use of basis functions for which the supports have different lengths. This method assumes that Rayleigh integral (6) is valid everywhere in the air, on and outside S (i.e., $\forall y \geq a(x)$). In this paper, we do not want to define the theoretical validity domain of this hypothesis, but we attempt to define, by means of convergence tests and for different surface profiles, the numerical applicability domain of the Rayleigh integral associated with our method.

3. METHOD OF RESOLUTION: METHOD OF MOMENTS

With the Rayleigh hypothesis, the Dirichlet boundary condition on S yields:

$$\begin{gathered}\frac{1}{2\pi}\int_{-\infty}^{+\infty} \hat{c}(\alpha)e^{-j\beta(\alpha)a(x)}e^{-j\alpha x}d\alpha = -s(x) \qquad \forall x \in \,]-\infty; +\infty[\\ \text{where } \; s(x) = E_t^{(0)}(x, y = a(x)) = 2j\sin(\beta_i a(x)) \times e^{-j\alpha_i x}\end{gathered} \quad (11)$$

Equation (11) is a Fredholm integral equation of the first kind that we must solve to obtain $\hat{c}(\alpha)$. The resolution is based on a "triangle/Dirac" moment method [3, 4]. Function $\hat{c}(\alpha)$ is decomposed over a basis of triangle expansion functions $\hat{b}_p(\alpha)$ with variable supports

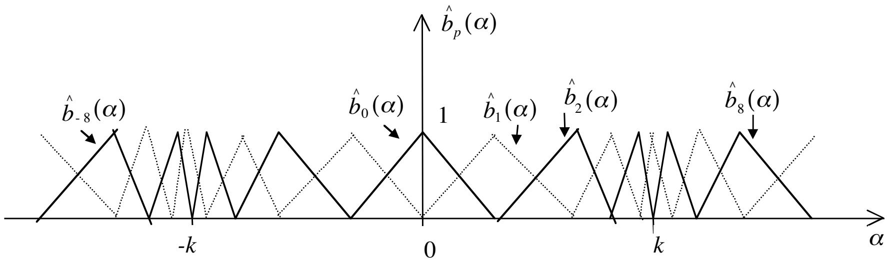

Figure 2. Functions $\hat{b}_p(\alpha)$ for $p = -8, -7, \ldots, 8$ with $Mc = 5$ (i.e., $\Delta\theta = 18°$).

(Fig. 2), which amounts to approximate $\hat{c}(\alpha)$ by a succession of lines:

$$\hat{c}(\alpha) = \sum_{p=-\infty}^{+\infty} c_p \hat{b}_p(\alpha) = \sum_{p=-\infty}^{+\infty} \hat{c}_p(\alpha_p)\hat{b}_p(\alpha) \tag{12}$$

$$\text{with} \qquad \hat{b}_p(\alpha) = \begin{cases} \dfrac{(\alpha - \alpha_{p-1})}{(\alpha_p - \alpha_{p-1})} & \text{if } \alpha \in [\alpha_{p-1}; \alpha_p] \\ \dfrac{(\alpha - \alpha_{p+1})}{(\alpha_p - \alpha_{p+1})} & \text{if } \alpha \in [\alpha_p; \alpha_{p+1}] \\ 0 & \text{else} \end{cases} \tag{13}$$

The α_p in (12) and (13) are obtained in sampling α with a constant angular interval $\Delta\theta$. For any integer p we have:

$$\text{if } |\alpha| \leq k\text{:} \begin{cases} \alpha_p = k\sin(p\Delta\theta) \\ \beta_p = k\cos(p\Delta\theta) \end{cases} \qquad \text{with} \quad p \in [-Mc; Mc]$$

$$\text{if } |\alpha| > k\text{:} \begin{cases} \text{if } \alpha > k\text{:} & \begin{cases} \alpha_p = k\cosh((p - Mc)\Delta\theta) \\ \beta_p = -jk\sinh((p - Mc)\Delta\theta) \end{cases} \text{with } p > Mc \\ \\ \text{if } \alpha < -k\text{:} & \begin{cases} \alpha_p = -k\cosh((p + Mc)\Delta\theta) \\ \beta_p = jk\sinh((p + Mc)\Delta\theta) \end{cases} \text{with } p < -Mc \end{cases} \tag{14}$$

Integer Mc, called “cut-off integer”, is the numerical parameter which sets the value of $\Delta\theta$:

$$\Delta\theta = \frac{\pi}{2Mc} \tag{15}$$

It should be noted that the lines which approximate $\hat{c}(\alpha)$ join the consecutive points $(\alpha_m; c_m)$. Moreover, as α approaches $\pm k$, the length of these lines when projected on the α-axis decreases. The motivation of such an approximation near $\alpha = \pm k$ is to take into strong consideration the physics of the problem; indeed, on both sides of the two cuts-off at $\alpha = \pm k$, the nature of the plane waves changes: the propagating waves are replaced by evanescent waves.

Equation (11) becomes:

$$\frac{1}{2\pi}\sum_{m=-\infty}^{+\infty}\left(J_m(x)c_m\right) + c(x) \approx -s(x) \qquad \forall x \in]-\infty; +\infty[$$

$$\text{with} \begin{cases} J_m(x) = \dfrac{I_m^{(1)}(x) - \alpha_{m-1} I_m^{(0)}(x)}{\alpha_m - \alpha_{m-1}} + \dfrac{-I_{m+1}^{(1)}(x) + \alpha_{m+1} I_{m+1}^{(0)}(x)}{\alpha_{m+1} - \alpha_m} \\ I_m^{(n)}(x) = \displaystyle\int_{\alpha_{m-1}}^{\alpha_m} \alpha^n \left(e^{-j\beta(\alpha)a(x)} - 1\right) e^{-j\alpha x} d\alpha \\ c(x) = TF^{-1}\left[\hat{c}(\alpha)\right] \end{cases} \tag{16}$$

After a positive Fourier transform of equation (16) and a projection over a basis of Dirac functions $\hat{\delta}(\alpha_q) = \hat{\delta}(\alpha - \alpha_q)$, the following matrix system is obtained:

$$[K]\vec{C} \approx -\vec{S} \text{ with } \begin{cases} [K]_{qm} = \dfrac{1}{2\pi} \times \hat{J}_m(\alpha_q) + \delta_{qm} \\ (\vec{C})_m = c_m \\ (\vec{S})_q = \hat{s}(\alpha_q) \end{cases} \quad \forall \text{ integer values } q \text{ and } m \tag{17}$$

where δ_{qm} is the Kronecker symbol, $\hat{J}_m(\alpha_q)$ and $\hat{s}(\alpha_q)$ are the Fourier transforms of $J_m(x)$ and $s(x)$ at $\alpha = \alpha_q$.

4. NUMERICAL APPLICATION

4.1. Numerical Parameters Mc and M

For the numerical calculation, the infinite sum of (16) is replaced by a finite sum with $2M + 1$ terms (with $M \geq Mc$). Integer M is the "truncation order". Thus, coefficients c_m are obtained by inverting a $2M + 1$ matrix (cf. (17)).

Integers Mc and M are the two numerical parameters of the method. For a given surface profile and a given incident wave, $2M + 1$ coefficients c_m are calculated. Among these coefficients, $2Mc + 1$ of them correspond to the amplitudes of the propagating waves and describe the asymptotic field or far field (8). The $2(M - Mc)$ remaining coefficients correspond to the evanescent waves; these waves contribute to describe the near field and take part in the couplings between the propagating waves.

Integer Mc sets the angular resolution $\Delta\theta$ (15). As Mc increases, $\Delta\theta$ decreases and the approximation of $\hat{c}(\alpha)$ by its decomposition over $\hat{b}_p(\alpha)$ (12) becomes more accurate. Thus approximation errors are smaller as Mc increases.

The consequence of the M^{th}-order truncation is the suppression of evanescent waves with a high spatial frequency in the Rayleigh integral. Indeed, integration variable α varies within $[-\alpha_{\max};\alpha_{\max}]$, where:

$$\alpha_{\max} = \alpha_M = k\cosh\left[\left(\frac{M}{Mc} - 1\right)\frac{\pi}{2}\right] \tag{18}$$

It is worth noticing that $\alpha_{\max}$ depends on ratio M/Mc. The proportion of evanescent waves is larger when M/Mc increases, so that the coupling phenomena are better described.

If our method is numerically stable, the accuracy of the results must increase with M and Mc. To illustrate this, we define two convergence tests for coefficients c_m, the first test as a function of M and the second one as a function of Mc. The aim is to determine if there is a pair $(Mc; M)$ which allows us to obtain stable values of c_m. Moreover, we must make sure that coefficients c_m verify the power balance criterion (10). In practice, for a pair $(Mc; M)$, the number of significant digits common to P_d and P_c is evaluated, i.e., the accuracy $\Delta P(M, Mc)$:

$$\Delta P(M, Mc) = -\log_{10}\left(\frac{|P_d(M, Mc) - P_c(M, Mc)|}{P_d(M, Mc)}\right) \tag{19}$$

4.2. Convergence Test as a Function of M

Mc is fixed and M is varied from $M_{\min} = Mc$ to $M_{\max}$. The test consists in calculating accuracies $\Delta c_0(M)$, $\Delta c_{Mc}(M)$, and $\Delta P_d(M)$ for all M:

$$\begin{aligned}\Delta c_m(M) &= -\log_{10}\left(\frac{||c_m(M)| - |c_m(M-1)||}{|c_m(M)|}\right)\\ \Delta P_d(M) &= -\log_{10}\left(\frac{|P_d(M) - P_d(M-1)|}{P_d(M)}\right)\end{aligned} \tag{20}$$

For each of the three magnitudes (c_0, c_{Mc} and P_d), the accuracy corresponds to the number of significant digits which remain unchanged when passing from $M-1$ to M. The method is numerically stable as a function of M if these accuracies increase with M.

In practice, let $[M_1; M_2]$ be the interval over which $\Delta c_0(M)$, $\Delta c_{Mc}(M)$ and $\Delta P_d(M)$ are greater than or equal to 2; we stipulate that all coefficients c_m of the propagating waves converge as a function of M if $M_2 = M_{\max}$ and $(M_2 - M_1) \geq Mc$. This criterion represents the convergence criterion $CM1$.

Moreover, power balance criterion (10) is evaluated for all M, by means of expression (19). Let $[M_3; M_4]$ be the interval over which $\Delta P(M, Mc) \geq 2$; we stipulate that the power balance criterion is verified if $M_4 = M_{\max}$ and $(M_4 - M_3) \geq Mc$. This criterion is the second convergence criterion $CM2$.

It is worth noticing that the value of $M_{\max}$ is imposed by the use of the discrete Fourier transform when evaluating $\hat{J}_m(\alpha_q)$ and $\hat{s}(\alpha_q)$ (cf. (17)). According to the Shannon criterion [23], in order to minimize the effects of the spectral aliasing, $M_{\max}$ must be such that:

$$2\alpha_{M_{\max}} < \frac{2\pi}{\Delta x} \tag{21}$$

i.e., according to (14) and (15):

$$M_{\max} = E\left[Mc + \frac{1}{\Delta\theta}\operatorname{arccosh}\left(\frac{\pi}{k\Delta x}\right)\right] \tag{22}$$

where Δx is the sampling interval of function $a(x)$, and $E[\ ]$ is the integer part.

The investigated deformation is a half cosine arch: $a(x) = (h/2)\cos(2\pi x/D)$ for $x \in [-D/4; D/4]$ with $h > 0$ and $l = D/2 = 0.625\,\lambda$. The surface is illuminated by a plane wave with a wavelength λ under incidence $\theta_i = 0°$. The sampling interval is $\Delta x = l/512$.

Table 1 gives the intervals $[M_1; M_2]$ and the relative errors on the power balance criterion for different heights h. Figures 3–5 illustrate the cases $h = 0.2\,\lambda$, $h = 1.1\,\lambda$ and $h = 230\,\lambda$. Variable $r_{\min}$ shown in Table 1 is the smallest integer value of ratio M/Mc for which the convergence criterion C$M1$ is verified:

$$r_{\min} = E[M_1/Mc] + 1 \tag{23}$$

Convergence criterion C$M1$ is verified $\forall h \leq 220\,\lambda$ with $\Delta x = l/512$ (cf. Table 1, Fig. 3a–c and 4a–c), i.e., for very large height to width ratios of the deformation. For each of these heights and with all ratios M/Mc such that $r_{\min} \leq (M/Mc) \leq (M_{\max}/Mc)$, convergence is ensured. Thus, there is at least one integer ratio M/Mc for which coefficients c_m are stable as a function of M (cf. Table 1). We notice that, for a given height, we find the same ratio $r_{\min}$ regardless of the chosen integer Mc ($Mc = 9$ or 27); thus the convergence of the coefficients as a function of M is not really influenced by the value of Mc. On the other hand, the more h increases, the slower coefficients

Table 1. Results of the convergence test as a function of M for different heights h of the 1/2 cosine arch with $l = 0.625\,\lambda$, $\theta_i = 0°$ and $\Delta x = l/512$.

				Convergence test of coefficients c_m				Power balance criterion	
h	h/l	Mc	M	$[M_1 ; M_2]$	Criterion CM1	r_{min}	E[M_{max} / Mc]	$\mid P_d - P_c \mid / \mid P_d \mid =$*	Criterion CM2
0.2 λ	0.32	9	$9 \to 47$	[18 ; 47]	verified	2	5	$3.3\ 10^{-3}$	verified
		27	$27 \to 142$	[28 ; 142]				$3.6\ 10^{-4}$	verified
0.5 λ	0.8	9	$9 \to 47$	[23 ; 47]	verified	3	5	$3.5\ 10^{-3}$	verified
		27	$27 \to 142$	[61 ; 142]				$4.5\ 10^{-4}$	verified
1.1 λ	1.76	9	$9 \to 47$	[29 ; 47]	verified	4	5	$7.59\ 10^{-2}$	not verified
		27	$27 \to 142$	[100 ; 142]				$4.07\ 10^{-2}$	not verified
10 λ	16	9	$9 \to 47$	[33 ; 47]	verified	4	5	$6.3\ 10^{-1}$	not verified
		27	$27 \to 142$	[107 ; 142]				$4.3\ 10^{-1}$	not verified
100 λ	160	9	$9 \to 47$	[37 ; 47]	verified	5	5	1	not verified
		27	$27 \to 142$	[115 ; 142]				$8.5\ 10^{-1}$	not verified
> 220 λ	> 352	9	$9 \to 47$		not verified	/	5		not verified

*the indicated relative error is calculated when stability of $\Delta P(M)$ is reached

c_m converge, and thus $r_{\min}$ is larger. This means that, as the height of the deformation increases, more and more evanescent waves must be taken into consideration to describe the scattering phenomenon.

For $h > 220\,\lambda$ with $\Delta x = l/512$, we observe a slow increase in the coefficient accuracies as a function of M (cf. Fig. 5), but the test stops before convergence criterion CM1 is satisfied. To continue the test, we must, for a fixed Mc, increase $M_{\max}$: this is possible provided Δx decreases (22). Results are convincing: for instance when $h = 230\,\lambda$ and $Mc = 9$ (cf. Fig. 5), criterion CM1 is not verified for $\Delta x = l/512$ ($M_{\max} = 47$ and $[M_1; M_2] = [37; 43]$), but is verified for $\Delta x = l/2048$ ($M_{\max} = 55$ and $[M_1; M_2] = [37; 55]$). Thus the validation of criterion CM1 depends on the sampling interval Δx.

In spite of the excellent convergence of the coefficients when h is large, the power criterion CM2 is verified only for $h \leq 0.5\,\lambda$ (cf. Table 1, Figs. 3d and 4d). $\forall h \leq 220\,\lambda$, we notice that accuracy ΔP becomes constant from a value of M which corresponds approximately to M_1 (cf. Fig. 3d and 4d). Here is the explanation of such a level: because of the decomposition of $\hat{c}(\alpha)$ over functions $\hat{b}_p(\alpha)$ (12), the calculation of the scattered power P_d involves an approximation error. As M increases, the accuracy of coefficients c_m increases but the approximation error on P_d does not decrease. For $M > M_1$, this approximation error becomes dominant and prevents any improvement in ΔP. This is why we observe a level. On the other hand, the approximation error on P_d must decrease as the angular interval $\Delta\theta$ decreases: we note that accuracy ΔP improves as Mc increases from $9(\Delta\theta = 10°)$ to

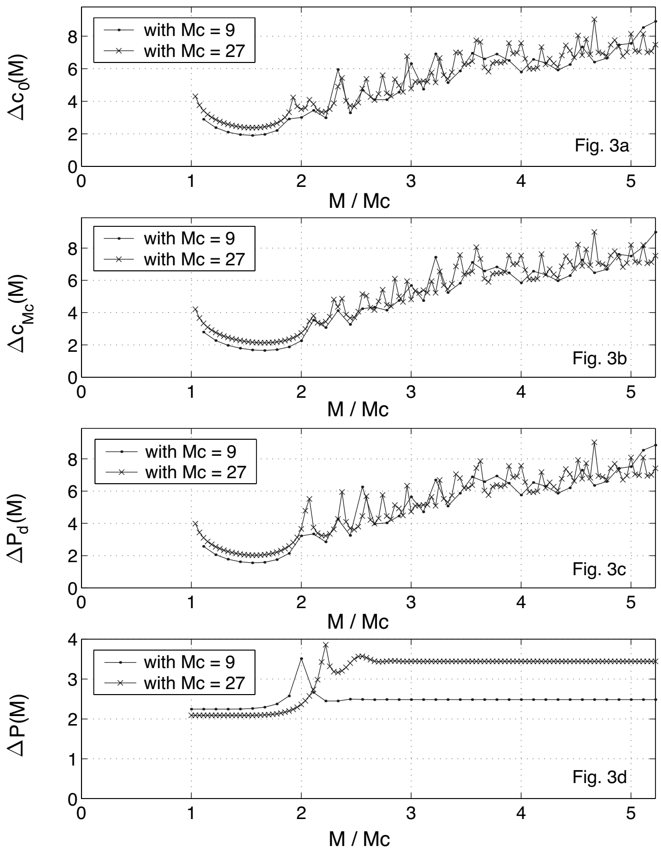

Figure 3. Accuracies $\Delta c_0(M)$, $\Delta c_{Mc}(M)$, $\Delta P_d(M)$ and $\Delta P(M)$ as a function of M/Mc for the 1/2 cosine arch with $l = 0.625\,\lambda$, $h = 0.2\,\lambda$, $Mc = 9$ and 27, $\theta_i = 0°$ and $\Delta x = l/512$.

27 ($\Delta\theta \approx 3.33°$) (cf. Table 1, Figs. 3d and 4d). Thus, we define a convergence test as a function of Mc to confirm this tendency for $Mc > 27$, therefore allowing the power balance criterion to be valid when $h > 0.5\,\lambda$.

4.3. Convergence Test as a Function of Mc

We make sure at first that the coefficients converge as a function of M and we choose an integer ratio M/Mc such that $r_{\min} \leq (M/Mc) \leq E[M_{\max}/Mc]$. We make Mc vary from $Mc_{\min} = 5$ to $Mc_{\max} = 100$. It is important to notice that the value of $\alpha_{\max}$ is not changed as Mc

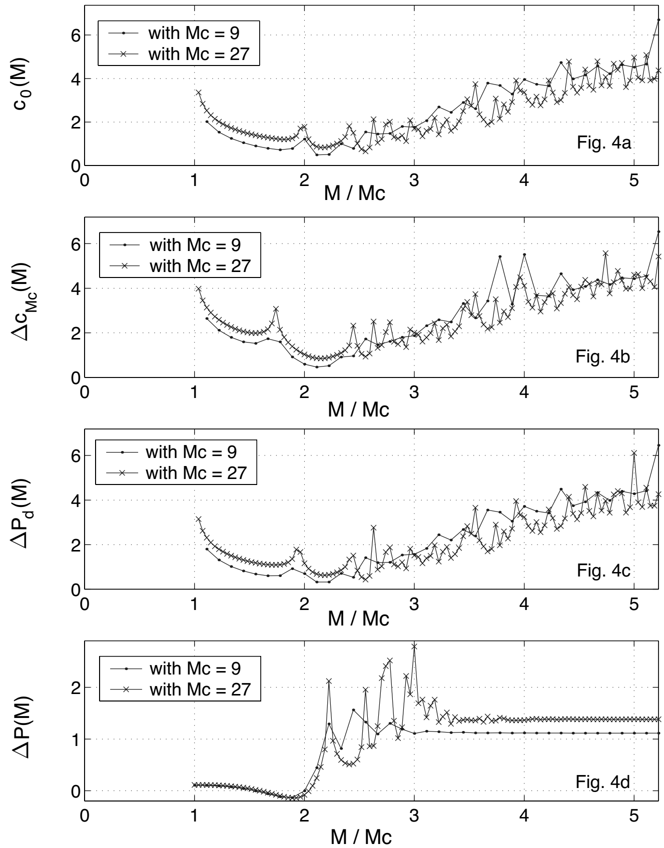

Figure 4. Accuracies $\Delta c_0(M)$, $\Delta c_{Mc}(M)$, $\Delta P_d(M)$ and $\Delta P(M)$ as a function of M/Mc for the 1/2 cosine arch with $l = 0.625\,\lambda$, $h = 1.1\,\lambda$, $Mc = 9$ and 27, $\theta_i = 0°$ and $\Delta x = l/512$.

varies because M/Mc is constant (cf. (18)). Therefore, the proportion of evanescent waves is constant regardless of Mc. On the other hand, the sampling of the interval $[-\alpha_{\max};\alpha_{\max}]$ is finer as Mc increases.

The test consists in calculating accuracies $\Delta c_0(Mc)$, $\Delta c_{Mc}(Mc)$, and $\Delta P_d(Mc)$ for each Mc:

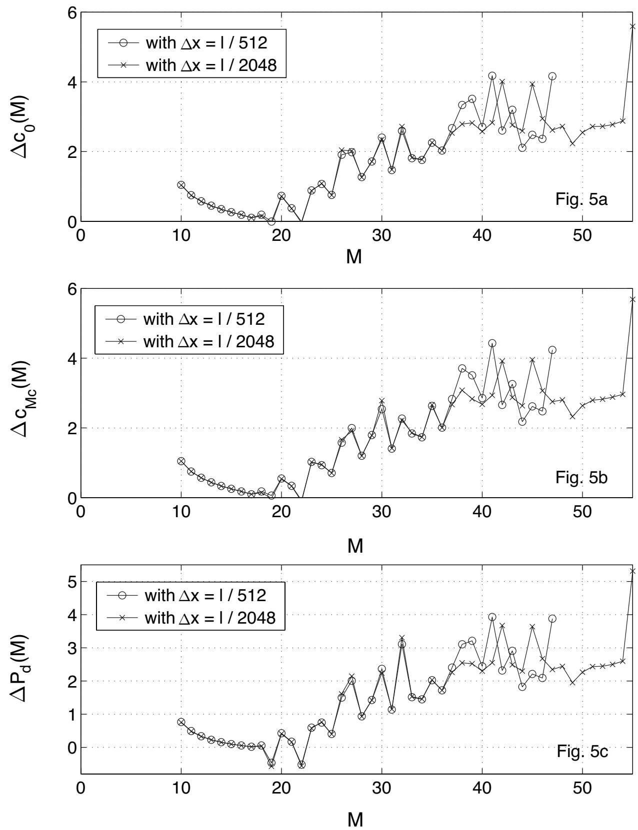

Figure 5. Accuracies $\Delta c_0(M)$, $\Delta c_{Mc}(M)$, and $\Delta P_d(M)$ as a function of M for the $1/2$ cosine arch with $l = 0.625\,\lambda$, $h = 230\,\lambda$, $Mc = 9$, $\theta_i = 0°$, $\Delta x = l/512$ and $l/2048$.

$$\Delta c_m(Mc) = -\log_{10}\left(\frac{||c_m(Mc)| - |c_m(Mc-1)||}{|c_m(Mc)|}\right)$$
$$\Delta P_d(Mc) = -\log_{10}\left(\frac{|P_d(Mc) - P_d(Mc-1)|}{P_d(Mc)}\right) \tag{24}$$

Each accuracy corresponds to the number of significant digits which remain unchanged from $Mc - 1$ to Mc.

Convergence criterion CMc1 is as follows : let $[Mc_1; Mc_2]$ be the interval over which $\Delta c_0(Mc)$, $\Delta c_{Mc}(Mc)$ and $\Delta P_d(Mc)$ are greater than or equal to 2; we stipulate that all coefficients c_m of the

Table 2. Results of the convergence test as a function of Mc for different heights h of the 1/2 cosine arch with $l = 0.625\,\lambda$, $\theta_i = 0°$ and $\Delta x = l/512$.

				Cv. test of the c_m		Power balance criterion		
h	h/l	M/Mc	Mc	$[Mc_1; Mc_2]$	Criterion CMc1	$[Mc_3; Mc_4]$	Criterion CMc2	$\lvert P_d - P_c \rvert / \lvert P_d \rvert =$ *
$0.2\,\lambda$	0.32	3	$5 \rightarrow 100$	[6 ; 100]	verified	[6 ; 100]	verified	$2.5\ 10^{-5}$
		4		[6 ; 100]		[6 ; 100]	verified	$2.6\ 10^{-5}$
$0.5\,\lambda$	0.8	4	$5 \rightarrow 100$	[6 ; 100]	verified	[5 ; 100]	verified	$6\ 10^{-7}$
$0.9\,\lambda$	1.44	4	$5 \rightarrow 100$	[11 ; 100]	verified	[27 ; 100]	verified	$1.5\ 10^{-4}$
λ	1.6	4	$5 \rightarrow 100$	[24 ; 100]	verified	[72 ; 92]	not verified **	$2.6\ 10^{-4}$
$1.25\,\lambda$	2	4	$5 \rightarrow 100$	[41 ; 100]	verified	/	not verified	$4.4\ 10^{-2}$
$3.5\,\lambda$	5.6	4	$5 \rightarrow 100$	[86 ; 100]	verified	/	not verified	1.03
$> 3.5\,\lambda$	> 5.6	4	$5 \rightarrow 100$	/	not verified	/	not verified	

*the indicated relative error corresponds to the smallest value over the interval $[Mc_1; Mc_2]$

**because $(Mc_4 - Mc_3) < (Mc_2 - Mc_1)/2$

propagating waves converge as a function of Mc if $Mc_2 = Mc_{\max}$.

Moreover, for each Mc, the power balance criterion is evaluated by calculating the accuracy $\Delta P(M, Mc)$ (19). Let $[Mc_3; Mc_4]$ be the interval over which $\Delta P(M, Mc) \geq 2$; we stipulate that power balance criterion is verified if $(Mc_4 - Mc_3) \geq (Mc_2 - Mc_1)/2$. This is the convergence criterion CMc2.

We consider the half cosine arch and the conditions of illumination defined in 4.2. Table 2 gives the intervals $[Mc_1; Mc_2]$, the intervals $[Mc_3; Mc_4]$ and the relative errors of the power balance criterion for different heights h. Figures 6–7 illustrate the cases $h = 0.2\,\lambda$ and $h = 1.1\,\lambda$.

Convergence criterion CMc1 is verified $\forall h \leq 3.5\,\lambda$ (cf. Table 2, Figs. 6a–c and 7a-c). We notice that the larger h, the larger Mc must be in order to reach the convergence. By a geometrical reasoning, we perceive that the larger h, the larger the interaction area (defined in Section 2); this widening in the "x-domain" requires a better sampling in the associated dual domain ("α-domain"), i.e., a smaller interval $\Delta\theta$, thus an increase in Mc.

When $h > 3.5\,\lambda$, convergence criterion CMc1 is not verified (cf. Table 2). Thus coefficients c_m are not stable, at least when $Mc \leq 100$. The maximum value of Mc was fixed at $Mc_{\max} = 100$ because the calculations for the test become too lengthy when $Mc > 100$.

Power criterion CMc2 is verified $\forall h \leq 0.9\,\lambda$ (cf. Table 2, Figs. 6d and 7d). Thus this criterion is much stricter than the criterion of convergence of the coefficients CMc1.

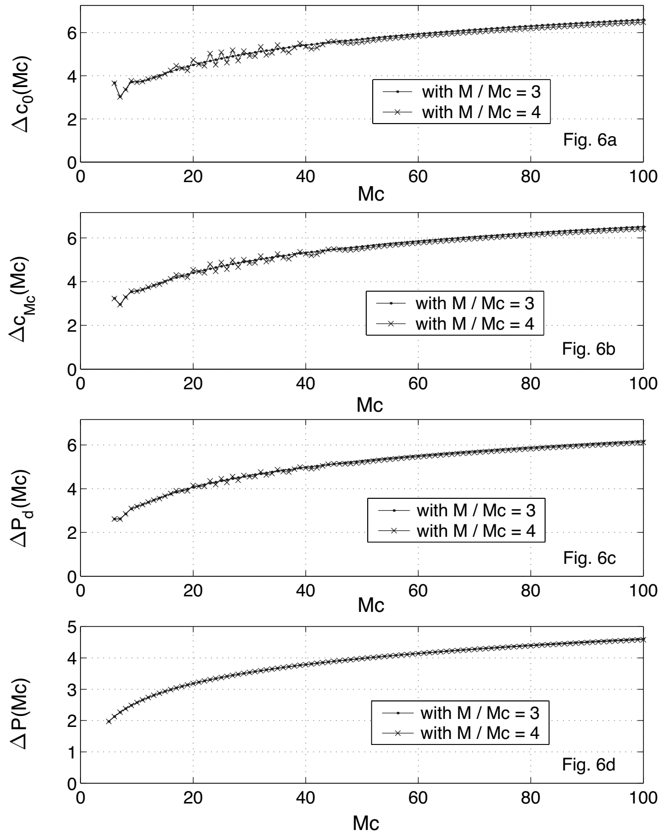

Figure 6. Accuracies $\Delta c_0(Mc)$, $\Delta c_{Mc}(Mc)$, $\Delta P_d(Mc)$ and $\Delta P(Mc)$ as a function of Mc for the 1/2 cosine arch with $l = 0.625\,\lambda$, $h = 0.2\,\lambda$, $M/Mc = 3$ and 4, $\theta_i = 0°$ and $\Delta x = l/512$.

4.4. Conclusion of the Two Convergence Tests

The convergence tests are applied to two coefficients ($c_{m=0}$ and $c_{m=Mc}$) and to the total scattered power P_d. Our convergence criterions $CM1$ and $CMc1$ suppose that the convergence of these three variables implies the convergence of the $2Mc+1$ coefficients of the propagating waves (the fact that the calculation of P_d uses these $2Mc+1$ coefficients is taken into account). In practice, for a few cases, the convergence tests have been applied to other coefficients c_m: results confirm that our hypothesis is realistic.

For the half cosine arch ($l = 0.625\,\lambda$) illuminated by a plane wave

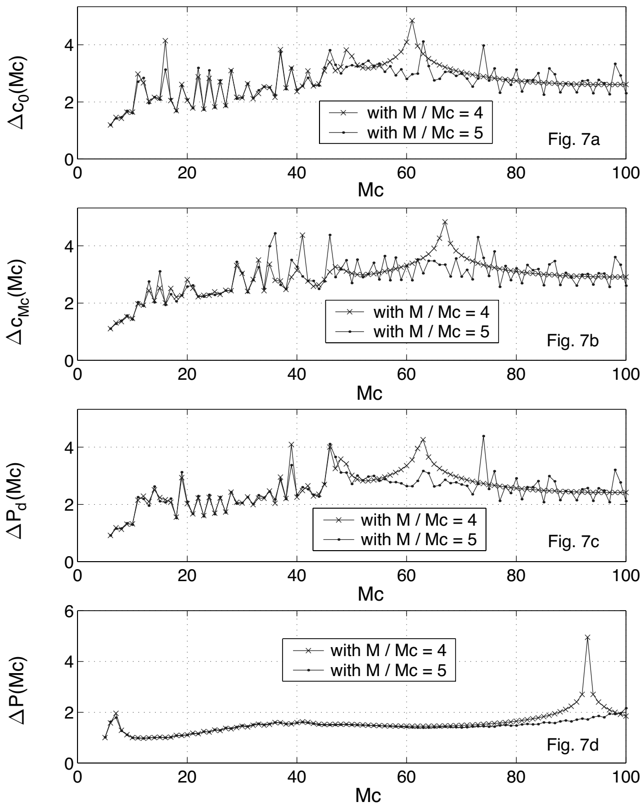

Figure 7. Accuracies $\Delta c_0(Mc)$, $\Delta c_{Mc}(Mc)$, $\Delta P_d(Mc)$ and $\Delta P(Mc)$ as a function of Mc for the 1/2 cosine arch with $l = 0.625\,\lambda$, $h = 1.1\,\lambda$, $M/Mc = 4$ and 5, $\theta_i = 0°$ and $\Delta x = l/512$.

under incidence $\theta_i = 0°$, the following conclusions can be drawn:

- for $0 < h \leq 0.9\,\lambda$ ($0 < h/l \leq 1.44$), the two convergence tests as a function of M and Mc are good and ensure the validity of the propagating coefficients c_m. Figure 8 shows the normalized scattering pattern $[dP_d(\theta)/d\theta]/\max[dP_d(\theta)/d\theta]$, obtained with the Rayleigh method and with a rigorous method for $h = 0.8\,\lambda$. The comparison is good (the reference method is based on Maxwell equations in covariant form written in a non-orthogonal coordinate system fitted to the surface profile [24, 25]). In this example, the computation time for the Rayleigh method (about 1 min.) is twenty times shorter than for the reference method (about 20 min.).

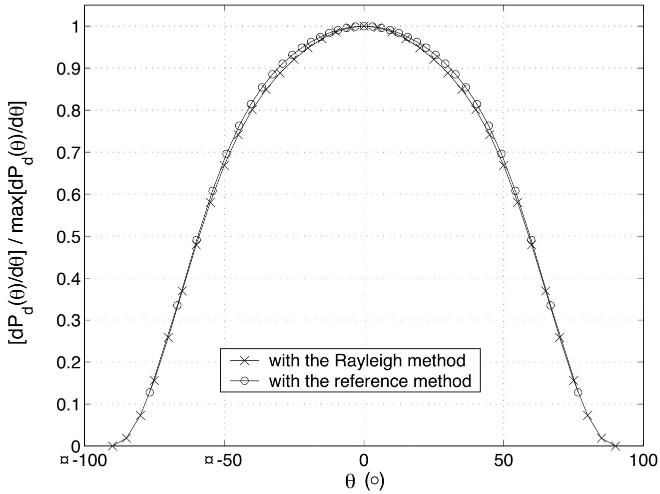

Figure 8. Normalized scattering pattern obtained with the Rayleigh method and the reference method for the 1/2 cosine arch with $l = 0.625\,\lambda$, $h = 0.8\,\lambda$, $\theta_i = 0°$ and $\Delta x = l/512$. (for the Rayleigh method, $Mc = 18$ and $M/Mc = 4$)

- for $0.9\,\lambda < h \leq 3.5\,\lambda$ $(1.44 < h/l \leq 5.6)$, coefficients c_m converge but the error on the power balance criterion is greater than 10^{-2}. The comparison with the reference method is not satisfactory.
- for $h > 3.5\,\lambda$ $(h/l > 5.6)$, coefficients c_m do not converge and the results are not reliable.

The test results are given for incidence $\theta_i = 0°$, but all the established conclusions remain valid regardless of the incidence angle.

Theoretical work shows that the Rayleigh method is valid for analytical profiles only. However, the half cosine arch used for the tests has a non-continuous derivative at two points ($x = \pm l/2$) and the proposed Rayleigh method yields good results in the far-field zone for perturbations, the amplitude of which is close to half the wavelength.

In the following paragraph, a case with an analytic profile is presented and we show that the numerical applicability domain of our method is wider than the theoretical validity domain.

4.5. Comparison with the Theoretical Limits

P. M. van den Berg and J. T. Fokkema have investigated analytically the validity of the Rayleigh hypothesis in the theory of scattering by a

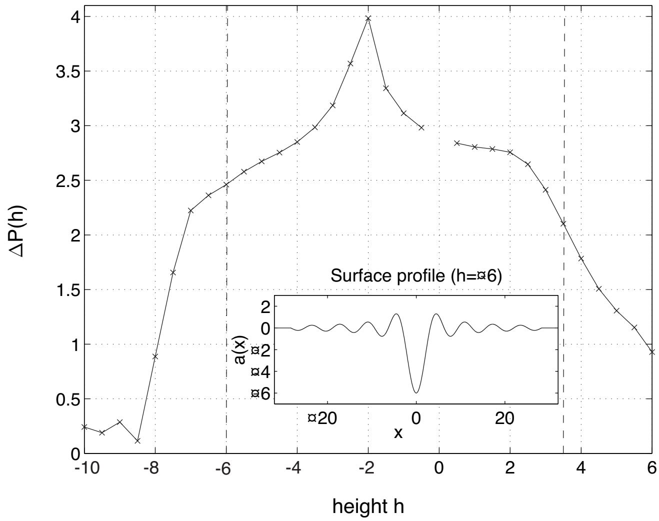

Figure 9. Accuracy of the power balance criterion $\Delta P(h)$ as a function of height h for $a(x) = h\sin(x)/x$ with $l = 6\,\lambda,\ \lambda = 3\pi,\ Mc = 18,\ M/Mc = 3,\ \theta_i = 0°$ and $\Delta x = \pi/256$. When $h = -7$ and $h = -6.5$, it can be noted that $\Delta P(M = 54,\ Mc = 18) \geq 2$. However, the obtained c_m values are not reliable because criterions $\mathrm{C}Mc1$ and $\mathrm{C}Mc2$ are not verified.

cylindrical perturbation in a plane surface [1]. They have established a procedure that enables us to know the validity of this hypothesis for surfaces whose profile can be described by an analytical function. For instance, they have demonstrated that for a surface described by $a(x) = h\sin(x)/x$ and illuminated by a plane wave, the Rayleigh hypothesis is valid when $-1.1161 < h < 0.98537$.

The numerical applicability domain of our method is evaluated for this surface: coefficients c_m are calculated for different heights and submitted to the two convergence tests (as is done in 4.2, 4.3 and 4.4). We choose $\lambda = 3\pi,\ \Delta x = \pi/256$ and $l = 6\,\lambda$. Figure 9 shows the accuracy of the power balance criterion $\Delta P(M = 54,\ Mc = 18)$ as a function of height h. Criterions $\mathrm{C}M1$, $\mathrm{C}Mc1$ and $\mathrm{C}Mc2$ are verified when $-6 \leq h \leq 3.5$ $(-0.64\lambda \leq h \leq 0.37\,\lambda)$. Thus the numerical applicability domain of our method for this surface is approximately 5.3 times wider than the theoretical validity domain of the Rayleigh hypothesis when $h < 0$ and about 3.5 times wider when $h > 0$. Both these ratios are of the same order of magnitude as the ratio obtained for the sinusoidal diffraction grating (for this grating, the theoretical validity domain is $\pi h/D < 0.448$ and the numerical applicability domain is $\pi h/D \lesssim 2$, thus a ratio of about 4.5).

4.6. Advantages of the Variable Supports of the Basis Functions

Our method is based on a method of moments with triangle basis functions $\hat{b}_p(\alpha)$, whose supports are variable (cf. (12), (13), (14) and Fig. 2). By comparison with a constant support, the choice of a variable support is advantageous with regard to the calculation time.

The basis of functions with constant support is defined as in (13), but with a constant sampling interval $\Delta\alpha$ for α and $\beta(\alpha)$:

$$\alpha_p = p\Delta\alpha \quad \text{and} \quad \begin{cases} \beta_p = \sqrt{k^2 - \alpha_p^2} & \text{if } |\alpha| \le k \\ \beta_p = -j\sqrt{\alpha_p^2 - k^2} & \text{if } |\alpha| > k \end{cases} \quad \text{with} \quad \Delta\alpha = k/Mc \tag{25}$$

where Mc is the "cut-off integer" and p is an integer varying from $-M$ to M.

We consider the half cosine arch defined in 4.2 with $h = 0.5\,\lambda$, $\theta_i = 60°$, $\Delta x = l/512$ and $Mc = 9$. Using the two kinds of support (variable and constant), the convergence test as a function of M is applied. The test results are shown in Table 3. Figure 10 shows accuracies Δc_0, Δc_{Mc}, ΔP_d and ΔP as a function of $\alpha_{\max}/k$ for the two kinds of support.

Table 3. Convergence test as a function of M with variable and constant support for the 1/2 cosine arch with $l = 0.625\,\lambda$, $h = 0.5\,\lambda$, $Mc = 9$, $\Delta x = l/512$ and $\theta_i = 60°$.

Support	M	M_1	α_{M1}/k	Power balance criterion		CPU time
variable	$9 \to 31$	25	≈ 8.2	stable over [26; 31]	$\lvert P_d - P_c \rvert / \lvert P_d \rvert \le 5.0\ 10^{-3}$ *	≈ 10.7 s
constant	$9 \to 198$	87	≈ 9.7	stable over [135; 198]	$\lvert P_d - P_c \rvert / \lvert P_d \rvert \le 6.6\ 10^{-3}$ *	≈ 608.9 s

*the indicated relative error is calculated when the stability of ΔP is reached

The behavior of accuracies Δc_0, Δc_{Mc}, ΔP_d and ΔP as a function of $\alpha_{\max}/k$ is similar with both supports. Convergence criterion C$M1$ is verified from $\alpha_{\max}/k = \alpha_{M1}/k \approx 9.7$ for the constant support and $\alpha_{\max}/k = \alpha_{M1}/k \approx 8.2$ for the variable support (Fig. 10). On the other hand, because the dependence between M and $\alpha_{\max}$ is linear for the constant support and exponential for the variable support (cf. (18)), integers M_1 which correspond to the obtained α_{M1}/k are 87 and 25, respectively, giving a ratio of about 3.5. The main consequence of

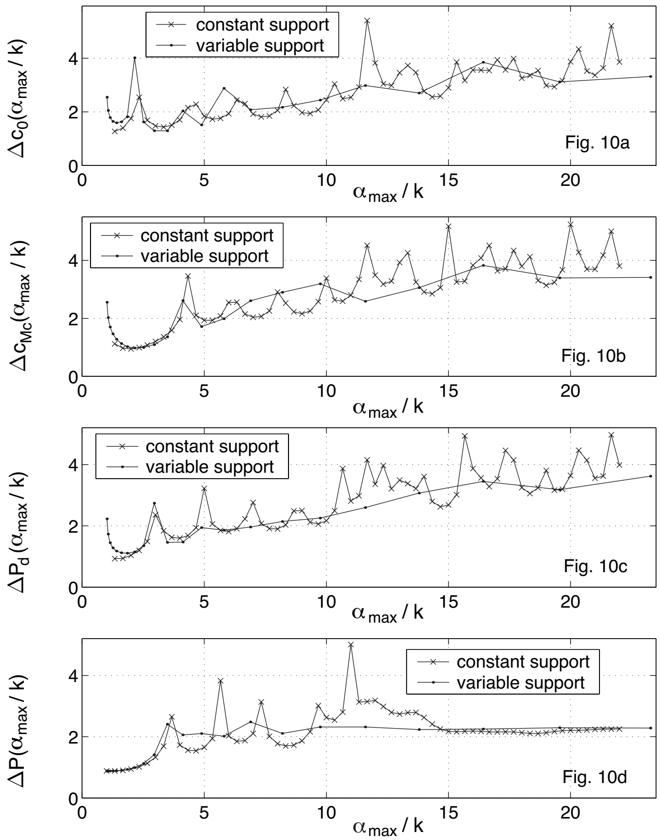

Figure 10. Accuracies Δc_0, Δc_{Mc}, ΔP_d and ΔP as a function of $\alpha_{\max}/k$ with variable and constant support for the 1/2 cosine arch with $l = 0.625\,\lambda$, $h = 0.5\,\lambda$, $Mc = 9$, $\theta_i = 60°$ and $\Delta x = l/512$.

this difference is the computation time: it takes about 57 times longer to execute the test with the constant support than with the variable support.

Thus, the two advantages of the variable support are the saving of time and the possibility to choose a very large $\alpha_{\max}$ without being limited by the computational capacity of computers.

5. CONCLUSION

A Rayleigh method giving the field scattered by a perfectly conducting plane surface with a local perturbation illuminated by a plane wave in $E_{//}$-polarization has been presented. Once the Rayleigh hypothesis is done, the scattered field is represented everywhere by a superposition of outgoing plane waves, whose amplitudes are given by function $\hat{c}(\alpha)$. A method of moments allows $\hat{c}(\alpha)$ to be obtained for $\alpha \in [-\alpha_{\max}; +\alpha_{\max}]$. Function $\hat{c}(\alpha)$ is expanded into a series of triangle basis functions $\hat{b}_p(\alpha)$, the supports of which are $[\alpha_{p-1}; \alpha_{p+1}]$. To compute the $2M+1$ expansion coefficients c_p, the Fourier transform of the boundary condition is used at $2M+1$ points α_p. The distribution of points α_p can be uniform (method with constant supports). In this case, the method is characterized by the spectral resolution $\Delta\alpha = k/Mc$ and by $\alpha_{\max} = M\Delta\alpha$. A non-uniform distribution of points α_p has been essentially studied (method with variable supports). In that case, the method is characterized by the angular resolution $\Delta\theta = \pi/(2Mc)$ and by $\alpha_{\max} = k \cosh[(M/Mc - 1)\pi/2]$. For a given pair of parameters $(Mc;\ M)$, this $\alpha_{\max}$ is greater than the $\alpha_{\max}$ of the uniform distribution. This implies (among other things) that, for the same accuracy on results, the method with variable supports requires shorter computation times.

The method has been numerically investigated in the far-field zone, by means of two convergence tests. For non-analytical profiles, the Rayleigh hypothesis is not valid. Nevertheless, we show that the proposed Rayleigh method gives reliable results for half cosine arch whose amplitude is close to half the wavelength. The results are stable and the power balance criterion is verified on significant intervals of truncation order M and cut-off integer Mc. Moreover, the comparison with the scattering patterns given by a rigorous method [24, 25] is good.

The numerical applicability domain in the far zone is much more extensive than the analytical validity domain. For example, with the profile $a(x) = h\sin(x)/x$, we show that the Rayleigh integral can be used with deformation amplitude about 3 times greater than the theoretical bound if $h > 0$ and about 5 times greater if $h < 0$ [1].

Thus, the proposed Rayleigh method is fully capable of accurately describing the far field produced by a very wide class of corrugated surfaces with reasonable CPU times by comparison with rigorous methods.

APPENDIX A.

A.1. Expressions of Scattered Fields $\vec{E}_d$ and $\vec{H}_d$ in the Far-Field Zone

In the far-field zone, the Rayleigh integral (6) is reduced to the only contribution of the propagating waves. With polar coordinates (r, φ) such that $x = r \sin\varphi$ and $y = r \cos\varphi$, equation (6) becomes [26]:

$$E_d(r,\varphi) = \frac{k}{2\pi} \sum_{n=-\infty}^{+\infty} \left[J_n(kr) e^{jn\varphi} e^{-jn\pi/2} \int_{-\pi/2}^{+\pi/2} \hat{c}(\theta) \cos\theta e^{-jn\theta} d\theta \right] \tag{A1}$$

where $J_n(r)$ is the Bessel function of order n, and:

$$e^{jkr\sin\gamma} = \sum_{n=-\infty}^{+\infty} J_n(kr) e^{jn\gamma} \tag{A2}$$

with $\gamma = \varphi - \theta - \pi/2$.

Function $\hat{c}(\theta)\cos\theta$ is analytically continued by the null function into the intervals $[-\pi; -\pi/2]$ and $[\pi/2; \pi]$. Then we make this analytical continuation periodic with period 2π. The periodic function $d(\theta)$ is obtained. $d(\theta)$ is expanded into a Fourier series:

$$d(\theta) = \sum_{n=-\infty}^{+\infty} d_n e^{jn\theta} \tag{A3}$$

with

$$d_n = \frac{1}{2\pi} \int_{-\pi}^{+\pi} d(\theta) e^{-jn\theta} d\theta = \frac{1}{2\pi} \int_{-\pi}^{+\pi} \hat{c}(\theta) \cos\theta e^{-jn\theta} d\theta \tag{A4}$$

Using (A3), (A4) and thanks to the behavior towards infinity of the Bessel functions (A5),

$$J_n(kr) = \sqrt{\frac{2}{\pi kr}} \left(e^{jkr - j(2n+1)\pi/4)} + e^{-jkr + j(2n+1)\pi/4)} \right) + O\left((kr)^{-3/2} \right) \tag{A5}$$

equation (A1) becomes:

$$\begin{aligned} E_d(r,\varphi) &= \sqrt{\frac{k}{2\pi r}} e^{jkr} e^{-j\pi/4} d(\varphi - \pi) + \sqrt{\frac{k}{2\pi r}} e^{-jkr} e^{j\pi/4} d(\varphi) + O\left(r^{-3/2}\right) \\ &= \sqrt{\frac{k}{2\pi r}} e^{-jkr} e^{j\pi/4} \hat{c}(\varphi) \cos\varphi + O\left(r^{-3/2}\right) \end{aligned} \tag{A6}$$

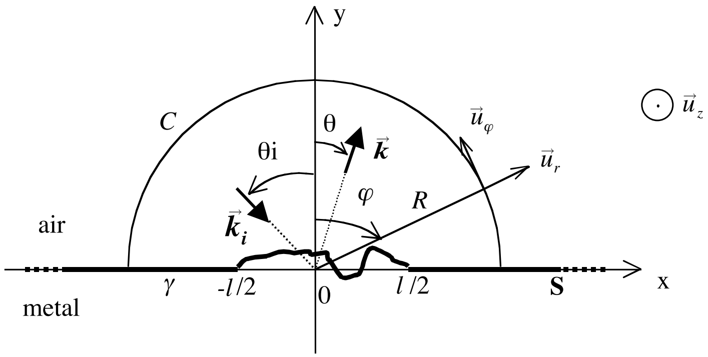

Figure A1. Integration contour for the second Green identity. According to our conventions, θ_i, θ and φ are positive here.

The expressions of the scattered fields $\vec{E}_d(r,\varphi)$ and $\vec{H}_d(r,\varphi)$ are obtained in the far-field zone:

$$\begin{cases} \vec{E}_d(r,\varphi) = \left(\sqrt{\dfrac{k}{2\pi r}} e^{-jkr} e^{j\pi/4} \hat{c}(\varphi) \cos\varphi + O\left(r^{-3/2}\right)\right) \vec{u}_z \\ \vec{H}_d(r,\varphi) = \dfrac{1}{Z} \vec{u}_r \wedge \vec{E}_d(r,\varphi) \\ \qquad = \left(-\dfrac{1}{Z}\sqrt{\dfrac{k}{2\pi r}} e^{-jkr} e^{j\pi/4} \hat{c}(\varphi) \cos\varphi + O\left(r^{-3/2}\right)\right) \vec{u}_\varphi \end{cases} \tag{A7}$$

A.2. Expression of the Power Balance Criterion

We consider the bounded contour $\Gamma = C \cup \gamma$ in Figure A1, where C is a half-circle centered at 0 of radius $R > l/2$, and γ is the part of surface S for $x \in [-R; R]$.

The total field $E_t(r,\varphi)$ is zero over γ. The second Green identity applied to $E_t(r,\varphi)$ on contour Γ yields [22, 26, 27]:

$$\mathrm{Im}\left[\int_C E_t(r,\varphi) \frac{\partial E_t^*(r,\varphi)}{\partial r} d\varphi\right] = 0 \tag{A8}$$

The total field $E_t(r,\varphi)$ is equal to the sum of the scattered field $E_d(r,\varphi)$ and the field without deformation $E_t^{(0)}(r,\varphi)$ (4). To calculate (A8), four integrals must be evaluated:

$$\mathrm{Im}\left[\int_{-\pi/2}^{+\pi/2} E_t^{(0)} \frac{\partial E_t^{(0)*}}{\partial r} d\varphi + \int_{-\pi/2}^{+\pi/2} E_t^{(0)} \frac{\partial E_d^*}{\partial r} d\varphi + \int_{-\pi/2}^{+\pi/2} E_d \frac{\partial E_t^{(0)*}}{\partial r} d\varphi + \int_{-\pi/2}^{+\pi/2} E_d \frac{\partial E_d^*}{\partial r} d\varphi\right] = 0 \tag{A9}$$

Using the asymptotic expression of $E_d(r,\varphi)$ (A7), the expression of $E_t^{(0)}(r,\varphi)$ (2), and the relations (A2)–(A5), we obtain:

$$\begin{aligned}
\mathrm{Im}\left[\int_{-\pi/2}^{+\pi/2} E_t^{(0)} \frac{E_t^{(0)*}}{\partial r} d\varphi\right] &= 0 \\
\mathrm{Im}\left[\int_{-\pi/2}^{+\pi/2} E_t^{(0)} \frac{\partial E_d^*}{\partial r} d\varphi\right] &= \frac{k}{r}\cos\theta_i[-\mathrm{Re}[c(\theta_i)] - \cos(2kr)\mathrm{Im}[c(-\theta_i)] \\
&\quad + \sin(2kr)\mathrm{Re}[c(-\theta_i)]] + O\left(r^{-2}\right) \\
\mathrm{Im}\left[\int_{-\pi/2}^{+\pi/2} E_d \frac{\partial E_t^{(0)*}}{\partial r} d\varphi\right] &= \frac{k}{r}\cos\theta_i[-\mathrm{Re}[c(\theta_i)] + \cos(2kr)\mathrm{Im}[c(-\theta_i)] \\
&\quad - \sin(2kr)\mathrm{Re}[c(-\theta_i)]] + O\left(r^{-2}\right) \\
\mathrm{Im}\left[\int_{-\pi/2}^{+\pi/2} E_d \frac{\partial E_d^*}{\partial r} d\varphi\right] &= \frac{k^2}{2\pi r}\int_{-\pi/2}^{+\pi/2} |\hat{c}(\varphi)|^2 \cos^2\varphi d\varphi + O\left(r^{-2}\right)
\end{aligned}$$

When identifying the $1/r$ terms, the power balance criterion can be established:

$$\frac{k}{4\pi Z}\int_{-\pi/2}^{+\pi/2} |\hat{c}(\varphi)|^2 \cos^2\varphi d\varphi = \frac{1}{Z}\mathrm{Re}\left[\hat{c}(\theta_i)\right]\cos\theta_i \tag{A10}$$

REFERENCES

1. Van den Berg, P. M. and J. T. Fokkema, "The Rayleigh hypothesis in the theory of diffraction by a perturbation in a plane surface," *Radio Sci.*, Vol. 15, 723–732, 1980.

2. Millar, R. F., "The Rayleigh hypothesis and a related least-squares solution to scattering problems for periodic surfaces and other scatterers," *Radio Sci.,* Vol. 8, 785–796, 1973.
3. Harrington, R. F., *Field Computation by Moment Methods,* Mc Millan, London, 1968.
4. Jones, D. S., *Methods in Electromagnetic Wave Propagation,* Clarendon Press, Oxford, 1979.
5. Petit, R. and M. Cadilhac, "Sur la diffraction d'une onde plane par un réseau infiniment conducteur," *C. R. Acad. Sci. B,* 468–471, 1966.
6. Millar, R. F., "On the Rayleigh assumption in scattering by a periodic surface," *Proc. Camb. Phil. Soc.,* Vol. 65, 773–791, 1969.
7. Millar, R. F., "On the Rayleigh assumption in scattering by a periodic surface - II," *Proc. Camb. Phil. Soc.,* Vol. 69, 217–225, 1971.
8. Van den Berg, P. M. and J. T. Fokkema, "The Rayleigh hypothesis in the theory of reflection by a grating," *J. Opt. Soc. Am.,* Vol. 69, 27–31, 1979.
9. Keller, J. B., "Singularities and Rayleigh's hypothesis for diffraction gratings," *J. Opt. Soc. Am. A,* Vol. 17, 456–457, 2000.
10. Van den Berg, P. M., "Reflection by a grating: Rayleigh methods," *J. Opt. Soc. Am. A,* Vol. 71, 1224–1229, 1981.
11. Hugonin, J. P., R. Petit, and M. Cadilhac, "Plane-wave expansions used to describe the field diffracted by a grating," *J. Opt. Soc. Am.,* Vol. 71, 593–598, 1981.
12. Wirgin, A., "Reflection from a corrugated surface," *J. Acoust. Soc. Am.,* Vol. 68, 1980.
13. Bagieu, M. and D. Maystre, "Waterman and Rayleigh methods for diffraction grating problems: extension of the convergence domain," *J. Opt. Soc. Am. A,* Vol. 15, 1566–1576, 1998.
14. Bagieu, M. and D. Maystre, "Regularized Waterman and Rayleigh methods: extension to two-dimensional gratings," *J. Opt. Soc. Am. A,* Vol. 16, 284–292, 1999.
15. Kleev, A. I. and A. B. Manenkov, "The convergence of point-matching techniques," *IEEE Trans. Antennas Propagat.,* Vol. 37, 50–54, 1989.
16. Christiansen, S. and R. E. Kleinman, "On a misconception involving point collocation and the Rayleigh hypothesis," *IEEE Trans. Antennas Propagat.,* Vol. 44, No. 10, 1309–1316, 1996.
17. Manenkov, A. B., "Comments on 'On a misconception involving point collocation and the Rayleigh hypothesis'," *IEEE Trans.*

Antennas Propagat., Vol. 46, 1765, 1998.

18. Maystre, D., "Electromagnetic scattering from perfectly conducting rough surfaces in the resonance region," *IEEE Trans. Antennas Propagat.,* Vol. AP-31, No. 6, 885–895, 1983.
19. Maystre, D. and J. P. Rossi, "Implementation of a rigourous vector theory of speckle for two-dimensional microrough surfaces," *J. Opt. Soc. Am.,* Vol. 3, 1276–1282, 1986.
20. Axline, R. M. and A. K. Fung, "Numerical computation of scattering from a perfectly conducting random surface," *IEEE Trans. Antennas Propagat.,* Vol. AP-26, No. 3, 482–488, 1978.
21. DeSanto, J. A., "Exact spectral formalism for rough-surface scattering," *J. Opt. Soc. Am. A,* Vol. 2, 2202–2207, 1985.
22. Petit, R., *Ondes Électromagnétiques en Radioélectricité et en Optique,* Masson (ed.), Paris, 1993.
23. Shannon, C. E., "Mathematical theory of communication," *Bell System Tech. J.,* Vol. 27, 379–423, 1948.
24. Afifi, S., "Propagation et diffraction d'une onde électromagnétique dans des structures apériodiques," Thése d'Université, Université Blaise Pascal de Clermont-Ferrand, France, 1986.
25. Benali, A., J. Chandezon, and J. Fontaine, "A new theory for scattering of electromagnetic waves from conducting or dielectric rough surfaces," *IEEE Trans. Antennas Propagat.,* Vol. 40, No. 2, 141–148, 1992.
26. Stratton, J. A., *Electromagnetic Theory,* McGraw-Hill Book Company, New York and London, 1941.
27. Kong, J. A., *Electromagnetic Wave Theory,* John Wiley and Sons, 1990.